Thin Solid Films 758 (2022) 139425

Contents lists available at ScienceDirect

Thin Solid Films

journal homepage: www.elsevier.com/locate/tsf

Realization and optimization of enhanced and spectral selective photoluminescence in size and phase controlled nanocrystalline Ga_2O_3 films made by pulsed laser deposition

Debabrata Das [a,*], Nanthakishore Makeswaran [a,b], Francelia Sanchez Escobar [a,c], Susheng Tan [d], C.V. Ramana [a,b]

[a] Centre for Advanced Materials Research (CMR), University of Texas at El Paso, 500W University Ave, El Paso, TX 79968, USA
[b] Department of Mechanical Engineering, University of Texas at El Paso, 500W University Ave, El Paso, TX 79968, USA
[c] Department of Metallurgical, Materials, and Biomedical Engineering, University of Texas at El Paso, 500W University Ave, El Paso, TX 79968, USA
[d] Department of Electrical and Computer Engineering, and Petersen Institute of NanoScience and Engineering, University of Pittsburgh, 3700 O'Hara Street, Pittsburgh, PA 15261, USA

ARTICLE INFO

Keywords:
β-Ga_2O_3 thin films
Pulsed laser deposition
Morphology
Nano-columnar structure
Photoluminescence
Band gap

ABSTRACTCT

Realization and optimization of the optical properties for tunable and/or enhanced emission characteristics is critical to further advance the field of optoelectronics, photonics, and electronics for extreme environment applications. While recent advancements made to realize high-quality single crystals of Ga_2O_3, an interesting material for electronics and optoelectronics, strategies to obtain enhanced functionality and desired optical properties in nanocrystalline Ga_2O_3 without needing to expensive epitaxial systems or quite cumbersome equipment or rare-earth dopants remains a challenging problem for further development. In this context we have demonstrated high yield spectral selective photoemission, from pulsed laser deposited (PLD) un-doped Ga_2O_3 thin films with extensive control over nanocrystalline growth. Structural, interfacial and morphological investigation reveals the formation of perfect nanocrystalline seed layer promoting further growth of compact nano-columns with nano-textured atop. Optical spectroscopy demonstrates the desired control over band-edge absorption and realization of ideal photo-transition in perfectly oriented nano-columnar PLD β-Ga_2O_3 films. Ellipsometry shows the growth parameters dependent evolution of refractive index over broad spectral range. The findings as presented and described here provide evidence for controlled growth and realization of nanocrystalline β-Ga_2O_3 for functional device applications in optoelectronics in addition to provide a platform to further explore their futuristic technological applications.

1. Introduction

Recently gallium oxide (Ga_2O_3) and related oxide compounds have been gaining immeasurable attention from the scientific and engineering community. Being extremely lucrative from structural, chemical, electronic and photonic properties viewpoint, it has the potential to thrust the current scientific advancement to the next level [1]. Owing to be a part of ultra wide band gap (E_g~ 4.8 eV) semiconductor family, it is material of choice for deep ultra-violate (UV) optoelectronic and photonic applications [2–9]. Next to diamond [10,11], Ga_2O_3 is well explored ultra wide band gap oxide material, and is the material of choice as a transparent semiconductor with multifunctional applicability. Ga_2O_3 has relatively higher breakdown field (~8 $MVcm^{-1}$) than diamond, which is beneficial for high power electronic device for the application in next generation futuristic automotive and energy sectors [12,13]. In addition to that, excellent thermodynamic and chemical stability of this oxide semiconductor opens the possibility for extreme environment applications, such as high temperature chemical sensors for industrial equipment and extraterrestrial electronic/optoelectronic/photonic transducers, etc. [14–16]. In view of these fascinating properties and phenomena, efforts have been directed to utilize Ga_2O_3 in numerous applications, namely deep UV-photodetectors/light emitting diodes (LEDs)/integrated photonics, high power electronic devices, high temperature transducers, magnetic memories, antireflective coatings, high-energy scintillators, luminescent phosphors, battery electrodes, super-capacitors, thin film transistors,

* Corresponding author.

https://doi.org/10.1016/j.tsf.2022.139425
Received 23 October 2021; Received in revised form 22 July 2022; Accepted 30 July 2022
Available online 3 August 2022

flexible electronic devices, neuromorphic devices, etc. [13,17-23].

Naturally, Ga_2O_3 shows six different structural polymorphs, such as α, β, γ, δ, ε, and κ [1]. The monoclinic β-phase is the most stable throughout the wide temperature range. In spite of the aforementioned technological benefits, fabrication of β-Ga_2O_3 based devices is extremely challenging. Anisotropic thermal conductivity through different crystal orientation and high residual strain formation during heteroepitaxial growth are mainly responsible for that [1,24]. Researchers tried various physical and chemical methods, such as chemical vapor deposition, Metal-organic chemical vapor deposition, vapor phase epitaxy, halide vapor phase epitaxy, molecular beam epitaxy, chemical bath deposition, Czochralski, edge defined film-fed growth, floating zone technique, sputtering, electrospinning, pulsed-laser deposition (PLD) etc., to demonstrate growth/fabrication of β-Ga_2O_3 and its alloys [6,8,13,20, 25-30]. Among all other processes, pulsed laser deposition is well explored due to its low cost noncomplex mechanism to produce relatively high quality epitaxial thin films and nanostructures. Due to simplicity and economics of the fabrication process, PLD grown Ga_2O_3 and alloys can be integrated into inexpensive transducers for daily routine applications.

Though β-Ga_2O_3 has been being admired for high power transistors and solar blind photodetectors, scientists paid a greater attention to the luminescence behavior of Ga_2O_3 for potential optoelectronic and photonic applications [28,30-35]. With increasing demand for revolutionary quantum computing and neuromorphic algorithm there is a constant demand for smart/biocompatible materials for specific optical transduction. That is how β-Ga_2O_3 and related complex oxides become very crucial from optical properties point of view. The photoemission from Ga_2O_3 is mainly dominated by intermediate energy states [28,30-35]. These quasi energy bands in between valence and conduction bands are formed due to donor-acceptor (DA) states, impurity levels and defect states. Few reports are there explaining partial exitonic nature of these transitions. External doping with metallic ions has also been studied quite extensively to tune the emission spectrum throughout visible region. Other ex situ defect engineering processes are there, such as ion implantation or femtosecond lased treatment [36,37]. Being a part of ultra wide band gap semiconductor family, this tunability of photoemission through the UV and visible regions opens up various futuristic technological aspects in optics, optoelectronics and photonics divisions. Recently we have reported green emission from close compact nanocolumnar undoped β-Ga_2O_3 thin film by controlling the nano-texture, phase and Ga-O vacancy states [28]. The in-situ incorporation of dopant atoms inside main matrix makes the fabrication complicated along with introduction of additional parasitic component into the host material. Assertively, tailoring of photoemission is always preferred by controlling the crystallinity, phase, texturing, defect density and topography by minute control over growth dynamics. This in-situ growth optimization is more economic and highly precise than other ex-situ processes, like ion implantation, rapid thermal annealing and laser annealing, while tailoring its structural, optical and electronic characteristics. In this context, here in this paper, we present an approach to obtain tunable nanocolumnar, undoped β-Ga_2O_3 thin film over the visible and UV-A spectrum. Detailed structural, nano-morphological, and optical characterization have been done thoroughly to understand the system perfectly, so that the study provides a strategy to further advanced technological applications of β-Ga_2O_3.

2. Materials and methods

2.1. Target synthesis

The PLD targets were prepared through two step solid state reaction process. Pure Ga_2O_3 powder (Sigma Aldrich) initially pulverized and then annealed at 1100°C for 12 h, to eliminate any organic contamination present in the material. Then the powder was grinded again and was mixed with Polyvinyl alcohol (the binding element), followed by pellet formation. The pellet was cylindrical in shape with 1 inch diameter and 0.15 inch thick. Finally, the pellet was sintered at 1450°C for 24 h to prepare the final PLD target.

2.2. Thin film and device fabrication

All the samples were fabricated through pre-optimized two-step growth process on Si (100) substrates. Initial background chamber pressure was 0.4 Pa. For all samples the substrate was precleaned with acetone-isopropanol-deionized water and was dried under continuous nitrogen flow. After that the sample was kept at 725 °C inside the growth chamber for 1 h before deposition process to get rid of any organic contaminants. The distance between substrate and target was 45 mm. A KrF excimer laser with 248 nm UV emission was used to ablate the ceramic Ga_2O_3 target. Initial 20 nm layer was grown with 1 Hz lased pulse frequency for better nucleation on Si substrate. Following the seed layer, active region was deposited with 10 Hz pulse frequency. Deposition time for seed and active layer were ~ 1 and 5 min, respectively. Also, substrate temperature (monitored using a thermocouple attached to it) was kept same throughout the deposition process. The deposition rate (~0.9–2 Å per laser pulse), oxygen partial pressure (66.6 Pa) and laser energy density (~3 J/cm^2) were optimized based on required structural and optical behavior of Ga_2O_3 films on Si substrate. Overall film thickness was varied from ~150 to 250 nm, depending on the substrate temperature. Fig. 1 shows the schematic of nanocolumnar β-Ga_2O_3 thin film on silicon substrate.

2.3. Characterization

The as grown samples were subjected to X-ray diffraction (XRD) measurement for structural and crystallographic characterization. Rigaku Smartlab diffractometer with Cu(Kα) source and HyPix 3000 high energy resolution 2D HPAD detector were used for XRD measurement in θ/2θ mode. Bare surface morphological signature of Ga_2O_3 thin films were characterized using FEI Magellan 400 scanning electron microscope (SEM) at 2 kV operating voltage and Nano surf atomic force microscope (AFM) system. Transmission electron microscopy (TEM) imaging was done on a Thermo Scientific (formerly FEI) system at 200 kV operating voltage. The specimens for TEM measurement were prepared using a FEI Scios focused ion beam following a standard TEM sample preparation convention with the help of Ga^+ ion as a source of liquid ion.

To understand the optical behavior and to extract the optical properties of Ga_2O_3 thin film on Si substrate, diffused reflectance spectroscopy was done by JASCO V-770 spectrometer with single monochromator and an optical resolution of 0.3 nm. The luminescence behavior was measured through photoluminescence (PL) spectroscopy measurement. Ti: sapphire laser along with 3rd harmonic generator was used for the photoexcitation of the samples and emitted photons were detected through 0.02 nm resolution monochromator, followed by followed by photomultiplier tube detector. Spectroscopic ellipsometry was employed to investigate the optical behavior of the as grown Ga_2O_3 samples on Si substrate. Ψ (azimuth) and Δ (phase) were determined at

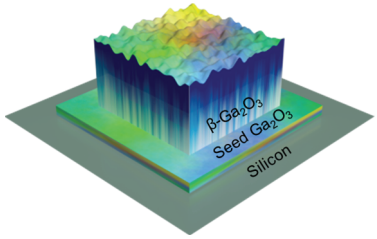

Fig. 1. Schematic of nanocolumnar β-Ga_2O_3 thin film on silicon substrate.

300 K under atmospheric condition over the range of 250–2000 nm with a resolution of 1 nm. The photon incident angle was kept at 75°, which is very near to the Brewster angle of Si substrate. Semilab SE-2000 was used for the measurement and Spectroscopic Ellipsometry. Analyzer v1.6.6.2 was used for analyzing and modeling of the spectroscopic data.

3. Results and discussion

Fig. 2 presents the X-ray diffraction (XRD) data, where the temperature dependent structural progression of nanocrystalline Ga_2O_3 thin film is visible. Note that XRD analyses can be used to understand the gradual evolution of crystal structure, cumulative strain, phase texturing and close compact nanocrystalline growth of Ga_2O_3 on Si. It is evident from the XRD data that Ga_2O_3 starts forming crystalline phases for substrate temperature $T_s \geq 600°C$. Below that all samples are in randomized amorphous structure. Such typical relation between substrate temperature and phase stabilization can be correlated with the pulse laser assisted growth dynamics of Ga_2O_3 thin film. The laser ablated plasma plume, embracing with highly energetic mixture of adatoms, molecules and ions, travels through oxygen environment and settles on the desired substrate. The partial oxygen medium inside the growth chamber supplements the anion deficiency of incoming adatoms and substrate temperature provides additional kinetic energy during initial nucleation and phase formation of Ga_2O_3 thin film. Lower substrate temperature ($T_s \leq 500°C$) cannot provide sufficient kinetic energy and results into amorphous Ga_2O_3 whereas higher substrate temperature facilitates highly textured nanocrystalline Ga_2O_3 thin film. Fig. 2a shows stable phase of β-Ga_2O_3 with C2/m space group for $T_s \geq 600°C$. The average crystallite size calculated from the XRD data is ~10 nm.

The degree of preferred orientation of nanocrystalline Ga_2O_3 films, grown at 700°C and 600°C, has been quantified, particularly the texture coefficient, from XRD data. The texture coefficient was calculated using [28]:

$$T_c = \frac{\frac{I_m(hkl)}{I_o(hkl)}}{\frac{1}{n}\sum_1^n \frac{I_m(hkl)}{I_o(hkl)}} \quad (1)$$

where Tc is the texture coefficient, I_m is the intensity of reflected X-ray beam from a particular plane, I_o is the intensity of the same plane form standard powder diffraction data and n is the total number of measured reflections. The texture coefficient variation is shown in Figs. 2b and 2c, respectively. Surely, the high temperature growth of Ga_2O_3 films is highly textured and reflects the cumulative effect of initial nucleation, surface diffusion/interdiffusion/outdiffusion and asymmetric thermal conductivity driven preferred nanocrystallization of Ga_2O_3. Overall, it shows the XRD peak corresponding to (−201), (−401), (−402), (−601), (−603), and (−801). 600°C substrate temperature results into random formation of parallel planes whereas 700°C makes it more oriented towards (−201) and related peaks. We believe lower formation energy and asymmetric thermal conductivity are responsible for this preferred growth of nanocrystalline Ga_2O_3 films. We have already shown similar growth mechanism of highly texture Ga_2O_3 thin film, based on high pressure zone-T Structure-Zone Model (SZM) [28].

In addition to XRD data, we employed the high-resolution transmission electron microscopy (TEM) to further assess the crystal quality, growth behavior, and surface/interface characteristics of PLD Ga_2O_3 thin films. Figs. 3-5 shows the temperature dependent evolution structure and interfacial characteristics of PLD Ga_2O_3 thin films. Cross sectional TEM image in accordance with selected area electron diffraction (SAED) pattern confirm the transformation of Ga_2O_3 phase from amorphous to compact highly textured nanocrystalline Ga_2O_3 thin film with increasing deposition temperature. The Ga_2O_3 thin film also exhibit the sharp interface along with the substrate. We have shown the low magnification TEM images for both amorphous (Fig. 3c, d) and nanocrystalline β-Ga_2O_3 thin film (Fig. 3a, b). Inset of Fig. 3a and 3d shows the crystalline and amorphous like SAED pattern for T_s= 700°C and 25

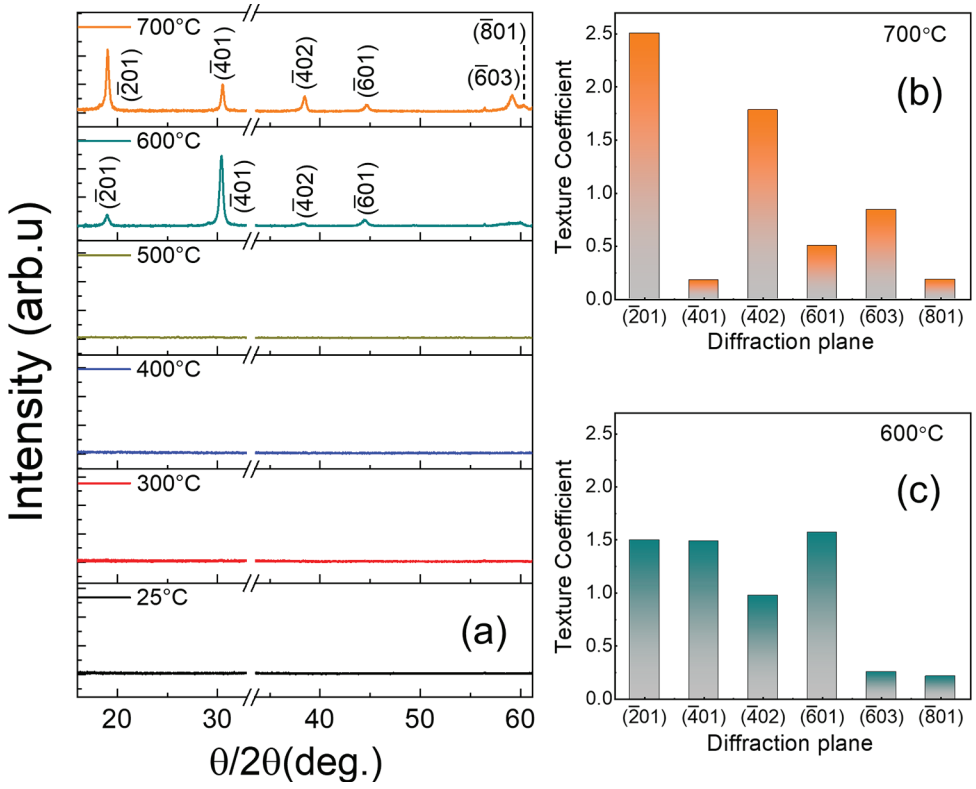

Fig. 2. (a) XRD pattern of nanocolumnar β-Ga_2O_3 thin film on silicon substrate with varying substrate temperature. (b-c) Texture coefficient of XRD peaks for 600°C and 700°C substrate temperature samples, respectively. The data presented clearly indicate the effect of substrate temperature on the growth behavior, crystal structure, and texture of Ga_2O_3 thin films.

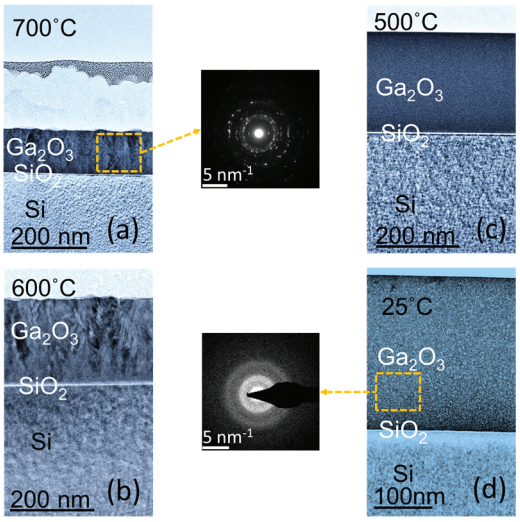

Fig. 3. (a-d) Low magnification cross sectional TEM image for PLD Ga_2O_3 thin films deposited at various temperatures. Inset is showing the SAED pattern of nanocrystalline β-Ga_2O_3 and amorphous Ga_2O_3 (top-down).

°C.

The laser pulse frequency, pulse number, and pulse power density have been kept same for all the depositions. As a result, with increasing substrate temperature, there is a clear reduction of the overall film thickness. With increasing substrate temperature, the adatoms get higher kinetic energy. Assertively, the rate of outdiffusion increases along with formation of close compact nanocolumnar Ga_2O_3 thin film which results into lower film thickness. Spectroscopic ellipsometry further verifies the trend of film thickness with increasing T_s. This is also evident from the TEM images at higher T_s values (Fig. 3a, 3b) that the active region is close compact overlapping nanocolumnar β-Ga_2O_3, grown on random nanocrystalline seed β-Ga_2O_3 layer. Fig. 4a-d shows the high magnification cross sectional TEM images to compliment the data shown in Fig. 3. Also, the inset of Fig. 4a, 4b and 4d depict the SAED patterns of nanocrystalline β-Ga_2O_3 seed layer, monocrystalline Si substrate and amorphous Ga_2O_3 seed layer for high and low T_s. Both the SAED patterns (4d and 4a inset) with high and low magnification confirms the temperature dependent growth of amorphous and

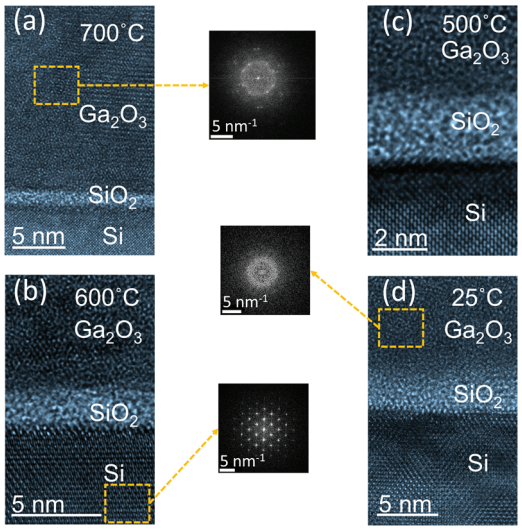

Fig. 4. (a-d) High magnification cross sectional TEM image for 25°C, 500°C, 600°C, 700°C samples showing Si/SiO_2/Ga_2O_3 interface, respectively. Inset is showing the SAED pattern of nanocrystalline β-Ga_2O_3 amorphous Ga_2O_3 and monocrystalline silicon (top-down).

nanocrystalline Ga_2O_3 seed layer and bulk thin film. Figs. 5a-d shows the high-resolution cross-sectional TEM-EDX (Energy dispersive X-ray spectroscopy) mapping of the corresponding samples. Low magnification images (Fig. 3) already confirm the overall abrupt interface between substrate and thin film, whereas Fig. 4 is portraying the atomistic nature of the interface that is further supported with EDX color mapping. For all the samples, the monocrystalline Si crystal structure is unharmed and is not showing any form of damage after the growth of Ga_2O_3 thin film. Similar pattern is found for SiO_2 interface throughout the temperature range. These confirm that there is no Ga assisted reverse etching of the substrate and no additional stimuli is not there during initial nucleation process at the beginning of the growth process. Additionally, the effective thickness of the intermediate SiO_2 layer reduces with increasing T_s, which is obvious due to increasing desorption and outdiffusion of SiO_2 from the bare substrate top layer.

Figs. 6 and 7 convey the 2D morphological signature of as deposited Ga_2O_3 thin film on Si substrate. Both scanning electron microscopy and atomic force microscopy have been employed to investigate the bare surface of amorphous and close compact nanocrystalline Ga_2O_3 thin film. SEM images with higher length scale have been showing the bulk surface evolution with increasing deposition temperature whereas AFM images are identifying the surface roughness and grain size distribution of nano-textured Ga_2O_3 thin film. Both the characterizations are conceding the structural characteristics, examined through XRD and XTEM analysis. Until 500°C, there is no signature of crystal formation. Overall film surface is flat without any significant features. Beyond that point, it starts showing crystallization and transformation from bulk amorphous Ga_2O_3 thin film into highly oriented nanocolumnar Ga_2O_3 thin film with compact nano-texturing atop. The gradual increment of surface roughness with increasing substrate temperature is due to transformation from random Ga_2O_3 molecules to nanocolumnar cluster of β-Ga_2O_3. The uncapped top surface of such growth front mimics the texture of collective semi-spheres with random size distribution. The nano-texture morphology of PLD deposited oxide thin films can be tailored by adjusting the in-situ growth parameters, such as laser power density, laser pulse frequency/energy, substrate temperature, substrate-distance/ angle between source and substrate, etc. Here we have used such typical parameters (mentioned earlier) to get a specific compact Ga_2O_3 nanoclusters for optimal photo-absorption through multiple in plane reflection and absorption method[38,39].

Spectroscopic ellipsometry is a powerful tool to understand the optical behavior of a given material through a specific wavelength range. Linearly polarized monochromatic light is subjected on the bare surface of thin film and the reflected beam is detected to estimate the complex reflectance ratio of the thin film. It is defined as following

$$\rho = R_P/R_S = \tan\psi \exp(i\Delta) \quad (2)$$

where R_S, R_P, ψ and Δ are complex reflection coefficient, amplitude component and phase difference respectively. The variation of ψ and Δ throughout the wavelength range can be simulated externally to estimate various intrinsic structural and optical parameters of the as grown

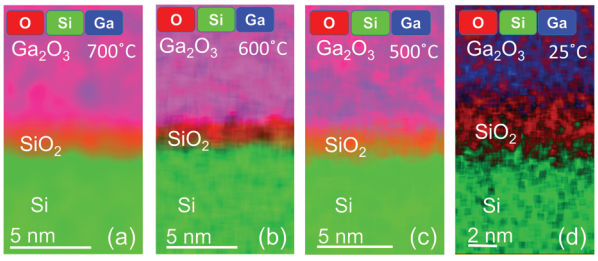

Fig. 5. (a-d) High magnification cross sectional TEM-EDX images PLD Ga_2O_3 thin films deposited under variable substrate temperatures. The images shows the Si/SiO_2/Ga_2O_3 interface for all the samples.

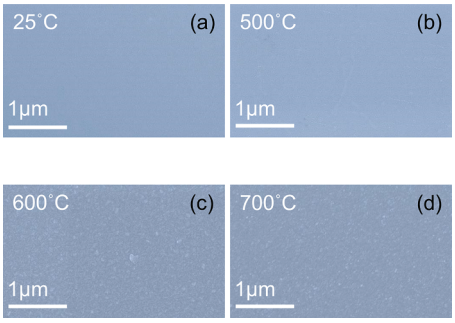

Fig. 6. (a-d) Low magnification SEM images of PLD Ga_2O_3 thin films deposited at various temperatures.

Ga_2O_3 thin film, such as film thickness, number of stacks, interface roughness, refractive index, extinction coefficient, etc. We have used Ga_2O_3/Si stacking model to simulate the measured spectrum to extract all possible physical and optical parameters of the given structure. The incident monochromatic light reflects and refracts according to the Fresnel relation and corresponding variation in the extracted beam is detected and simulated externally with the help of Cauchy dispersion law. This fitting model has been quite accurate to extract the inherent features of various high band gap oxide semiconductors. The model to calculate refractive index is shown below.

$$n = A + \frac{B}{\lambda^2} + \frac{C}{\lambda^4} \tag{3}$$

Here n is the refractive index as a function of wavelength. A, B and C defines the value of n in long (λ→∞), middle (vis) and short (UV) wavelength range respectively. Fig. 8a and b show the representative ψ and Δ spectra for nanocrystalline and amorphous Ga_2O_3 thin film. The measured and simulated data are in good agreement and is evident from both figures. Assertively, the higher number of fringes in amorphous sample is confirming the higher thickness for lower temperature samples.

The simulated refractive index patterns ate shown in Fig. 9a and b for PLD Ga_2O_3 thin films deposited at different substrate temperatures. The decreasing nature of film thickness (Fig. 9b) along with increasing substrate temperature is already discussed in previous section. The nature of the refractive index (n) spectrum is reflecting the optical behavior of the corresponding Ga_2O_3 films. For shorter wavelength, near the actual optical band gap of the given material, the amorphous films are showing higher values of n than that in nanocrystalline β-Ga_2O_3 films. Due to structural non-uniformity along with random orientation of nanoscale unit cells reduce the effective group velocity of light through the amorphous Ga_2O_3 films. This results into higher values of n. Whereas, nano-textured Ga_2O_3 thin films with superior crystalline quality promote the increasing group velocity of light through close compact mnanocolumnar Ga_2O_3 thin film and reflect into reduced value of n. Additionally, it is important to notice that for long wavelength (> 600 nm) the amorphous and nanocrystalline Ga_2O_3 films behave differently. The rate of change of n with increasing wavelength is relatively higher in amorphous Ga_2O_3 films. Whereas nanocrystalline films show no significant changes in this wavelength range. We believe drastic transformation, before and after 500°C, of crystalline nature is responsible for this typical behavior.

The Si substrate is opaque in UV–vis region, so transmission or absorption spectroscopy is not possible. Therefore, the optical absorption of amorphous and nanocrystalline Ga_2O_3 thin films on Si substrate was measured through indirect diffused reflectance spectroscopy. The measured spectral response then converted into Kubelka-Munk (K-M) function which is proportional to the absorption coefficient of the thin film. The K-M function is derived as following [40]:

$$F(R) = \frac{(1-R)^2}{2R} \tag{4}$$

Here, F(R) and R are the kubelka-Munk function and reflectance, respectively. Similarly, the Tauc plot was also modified by replacing the absorption coefficient with K-M function. The actual and modified Tauc equation are shown below.

$$\alpha \times h\upsilon = A\left(h\upsilon - E_g\right)^n \tag{5}$$

$$F(R) \times h\upsilon = A\left(h\upsilon - E_g\right)^n \tag{6}$$

Here, α, h, υ, E_g, F(R), and A represents absorption coefficient, Planck's constant, incident photon frequency, optical band gap, kubelka-Munk function, and fitting constant respectively. We have used $n = 1/2$ for the direct band optical transitions in Ga_2O_3 thin film. Figs. 10 and 11 show the corresponding Tauc plots and calculated band gaps of all as grown Ga_2O_3 samples, respectively. It is evident (Fig. 11) that the optical band gap shows an increasing trend with substrate temperature. Starting with 4.01 eV for room temperature deposition, the close compact nanocolumnar Ga_2O_3 films, grown at 700°C, is showing an optical band gap of 4.83 eV. This band gap value is comparable to the as reported

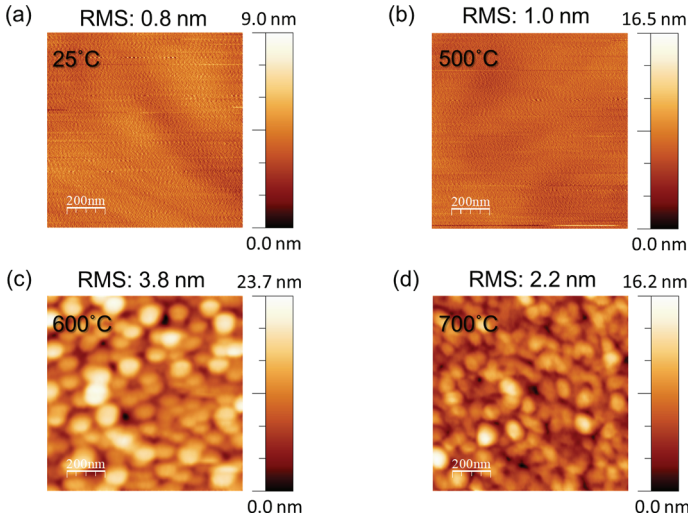

Fig. 7. (a-d) High magnification 3D AFM morphology images of PLD Ga_2O_3 thin films deposited at various temperatures. The morphology changes in Ga_2O_3 thin films as a function of deposition temperature are evident in these images.

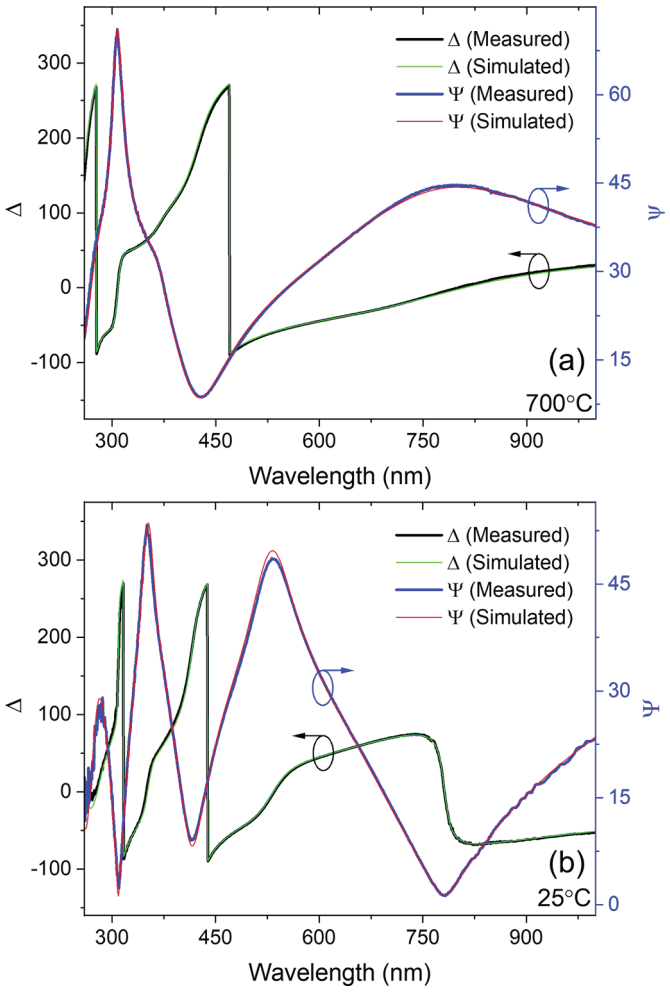

Fig. 8. (a, b) Measured and simulated psi, delta spectra for PLD Ga_2O_3 thin films deposited at 700°C and 25°C samples, respectively.

bulk β-Ga_2O_3. During the growth of Ga_2O_3 thin films under lower substrate temperature ($T_s \leq 500$ °C), incoming laser ablated adatoms did not get sufficient kinetic energy. Surely the grown amorphous material suffers from crystalline defects, interstitial trap states, surface states, etc. and deviates the band edge absorption from its ideal value. Whereas high substrate temperature results into good quality nanocolumnar Ga_2O_3 thin film, without any exploitative structural and electronic component, and shows a band gap closer to the ideal value.

The luminescence behavior of as-grown Ga_2O_3 thin films were investigated through room temperature photoluminescence spectroscopy and the data are shown in Fig. 12a. Though, we have excited the samples with photons having higher energy value than optical band gap of the samples, there is no signature of band to band transition. All of them are showing multimodal behavior, but of reduced energy than actual band gap. These are from Ga-O vacancy states (V_O, V_{Ga}, V_{Ga}-V_O), which form secondary quasi states between valence and conduction band of β-Ga_2O_3 [31,32,41]. Irrespective of its amorphous/nanocrystalline behavior, there are potential direct electron-hole recombination. It's true that randomized amorphous samples, grown at lower substrate temperature, show relatively lesser luminescence intensity, whereas textured nanocolumnar samples are having at least ~25-30 fold higher emission intensity. This particular feature can be correlated with the aforementioned structural and compositional behavior of the as grown samples. Nanocrystalline Ga_2O_3 thin films are having lesser parasitic defects whereas amorphous materials are very prone to defect formation [28]. As a result, with increasing defects, lower substrate temperature fabrication process reduces the overall luminescence intensity. Also, there is a clear blue shift of the peak spectrum with increasing substrate temperature. Room temperature and 300°C are showing green through red emission, but green emission become dominant with increasing substrate temperature. From 400°C, there is a significant blue spectrum but green is still dominating. As we increase the temperature further, the overall signal gets blue-shifted and for 700°C it shows a distinct UV-A peak. This kind of typical behavior is due to interplay between shallow and deep level energy states which can be tailored through controlled growth process [28,31,32,41].

Fig. 12b is depicting a schematic of steady state photo generated carrier dynamics [28]. The multicolor horizontal band is representing the inter band distribution of energy states. The excitation of carriers is from valance to conduction band. From there direct and indirect relaxation start. Phonon plays an important role indirectly in carrier transitions to its suitable energy states before recombination. Diagonal curved arrows are representing phonon assisted transitions. Multicolor broad downward arrow is showing the direct transition where we get actual photon emission. The typical color combination is chosen to represent the multimodal behavior of the emission spectrum which can be controlled with external probes during the growth process. The gray vertical curved arrow, pointing downwards through few dash lines, is reflecting the effect of defect state. There is no effective photon emission, so represented as dark color. Either excited carriers become trapped inside those trap state or they just hop through those states through phonon exchanging process. As an active optoelectronic material for LED application, emitting in visible spectrum, these parasitic states are not desired and can be reduced with higher growth temperature and controlled growth conditions.

To investigate the room temperature recombination dynamics of photogenerated carriers, Transient PL has been done on as grown samples. Only 600°C and 700°C samples are showing significant response. The samples with $T_s \leq 500$°C have shown very low intensity and the

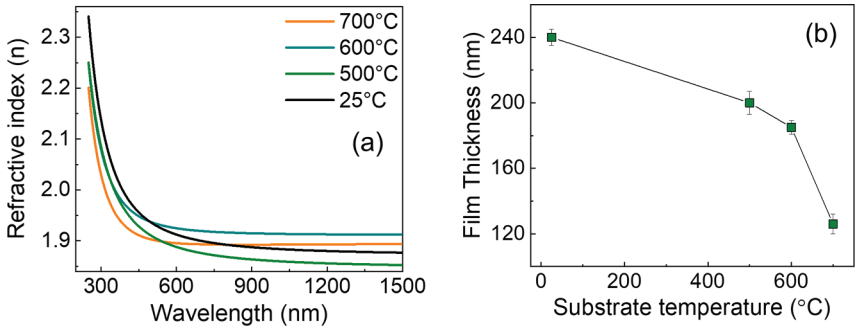

Fig. 9. (a) Wavelength dependent refractive index for amorphous and nanocolumnar β-Ga_2O_3 films grown by PLD. The data shown are for PLD Ga_2O_3 thin films deposited at various temperatures. (b) The variation of PLD Ga_2O_3 film thickness with deposition temperature, The data shown in is calculated film thickness from SE measurements.

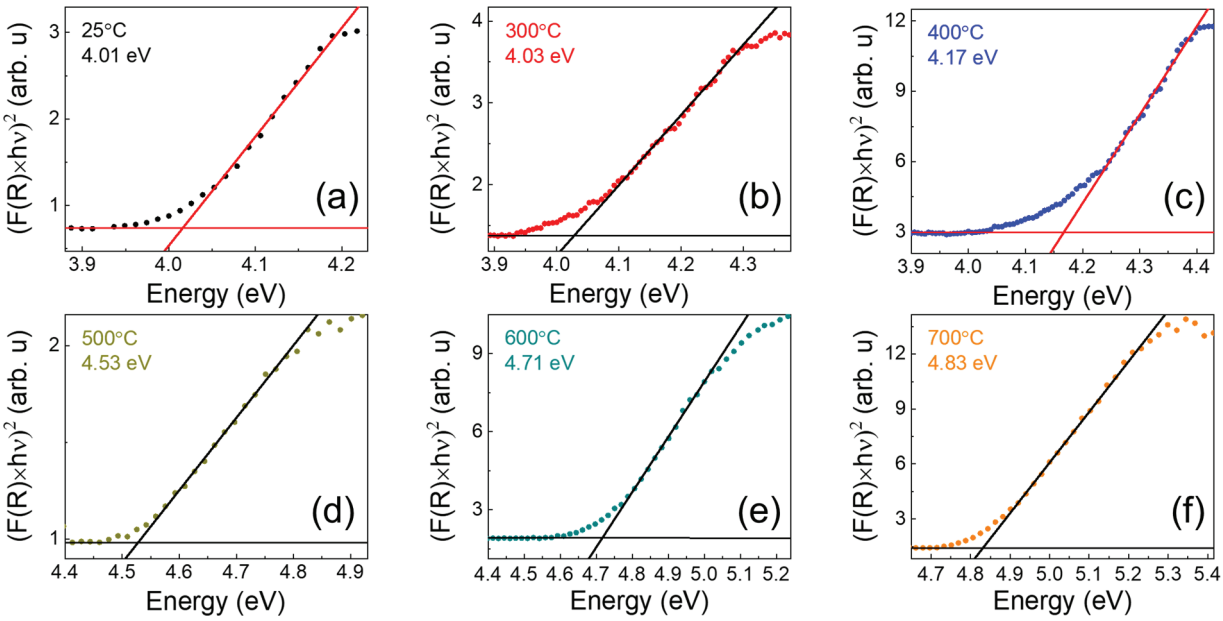

Fig. 10. (a-f) Tauc plots and calculated band gaps from diffused reflectance measurement of amorphous Ga_2O_3 and nanocrystalline β-Ga_2O_3 films deposited at variable substrate temperatures.

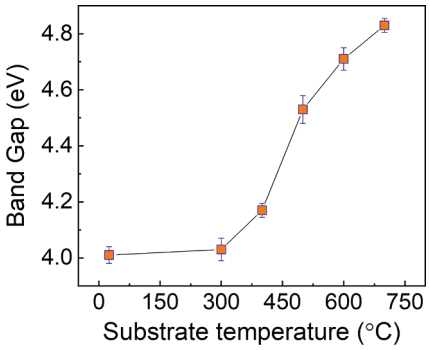

Fig. 11. Band gap variation with deposition temperature of PLD Ga_2O_3 thin films. The difference as well as the trend can be noted for amorphous Ga_2O_3 versus nanocrystalline β-Ga_2O_3 films grown various substrate temperatures.

transient data is not reliable due to overwhelming signal to noise ratio. Fig. 13a and 13b are showing the transient PL data for 600°C and 700°C samples. The data is fitted with double exponential decay function [42] which gives two corresponding time constants; τ_1, τ_2. The initial time constant τ_1 varies between ~400–500 ps, whereas the second time constant τ_2 shows a little higher value; ~1.5–2.4 ns. We believe that the faster component τ_1 is reflecting the decay time for non-radiative recombination of carriers and the slower component τ_2 is representing the radiative transitions[42]. The values corresponding to slower and faster decay component is in good agreement with the reported values for high band gap oxide semiconductors[43,44].

The sample with 700°C substrate temperature is showing a typical PL spectrum. Starting from UV-A band it is extended until red wavelength, covering almost all the significant regions of solar spectrum. It's true that the ratio of different bands is not quite similar to the actual solar spectrum, but can be tailored with pre-optimized growth conditions. Even we can demonstrate a white light source with proper doping incorporation into the system along with desired growth parameters. Typically, the asymmetric thermodynamic orientation during the growth of compact β-Ga_2O_3 nanocolumnar structure along with selective nucleation of incoming adatoms make the growth of defect free β-Ga_2O_3 more challenging. But, we have demonstrated the potential of precisely controlled growth to get desired structural, morphological and optical behavior. Moreover, the typical luminescence behavior makes this growth strategy more demanding for further broadband optoelectronic and photonic applications by demonstrating tunable luminescence without any additional dopant and needs further follow up to optimize for specific technological applications.

4. Summary and conclusions

We have performed detailed studies on the film growth, nanostructuring, surface/interface morphology, optical and optoelectronic properties and performance, and demonstrated a low-cost pulsed laser deposition to manifest Ga_2O_3 thin films with controlled structural and optical/optoelectronic behavior. Starting with amorphous Ga_2O_3 at low substrate temperature, we have established close compact nanocolumnar Ga_2O_3 thin films with nano-textured atop. Structural, morphological and interfacial characteristics reviles the formation of nanocrystalline seed layer, promoting the growth of overlapping nanocolumns with textured bare surface for efficient light trapping. Optical behavior reflects the band edge absorption near to the ideal value whereas extensive tunability has been observed in luminescence spectrum. Intermediate quasi band assisted broad emission, partially mimicking the solar spectrum, from such ultra high band gap metallic oxide semiconductor opens up a potential smart material for optoelectronic and photonic applications. Moreover, absence of any parasitic dopant, to manifest the desired luminescence outcome, makes this strategy more intuitive to the science community for further implantation into technological advancement.

CRediT authorship contribution statement

Debabrata Das: Conceptualization, Data curation, Formal analysis, Software, Writing – original draft, Writing – review & editing. **Nanthakishore Makeswaran:** Formal analysis, Writing – original draft. **Francelia Sanchez Escobar:** Methodology, Software, Investigation. **Susheng Tan:** Investigation, Supervision. **C.V. Ramana:** Supervision, Project administration, Funding acquisition, Writing – review & editing.

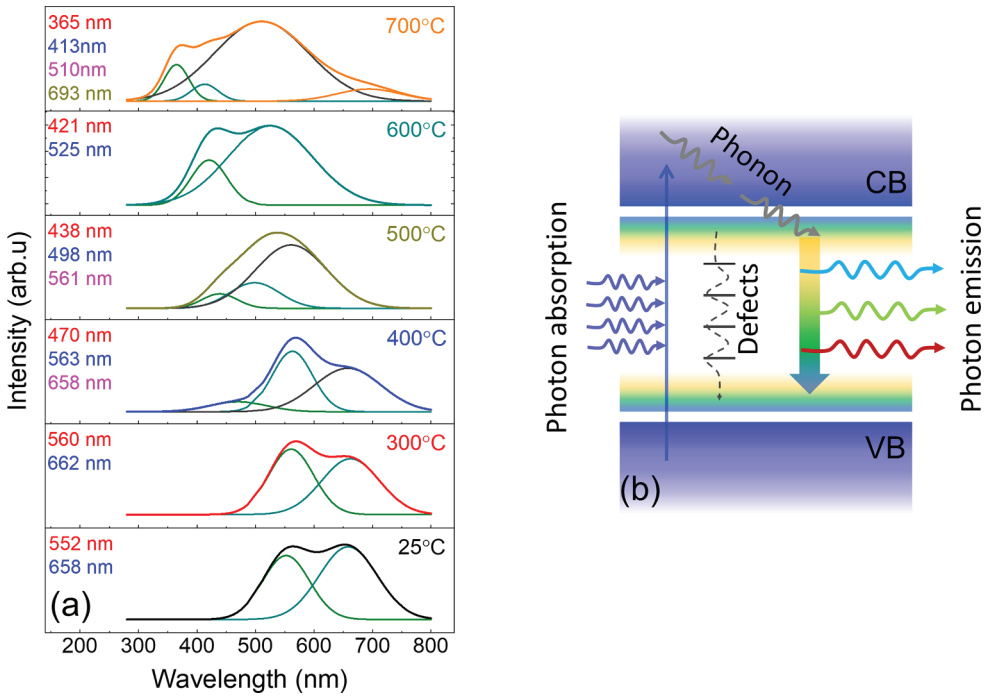

Fig. 12. (a) Room temperature PL spectrum of amorphous Ga_2O_3 and nanocrystalline β-Ga_2O_3 films made by PLD at different substrate temperatures. (b) Conceptual diagram explaining steady state carrier transitions inside nanocrystalline β-Ga_2O_3.

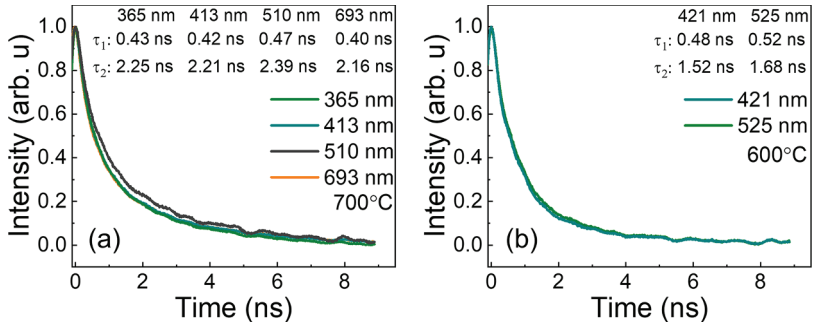

Fig. 13. (a, b) Room temperature TRPL spectrum of nanocrystalline β-Ga_2O_3 films grown at 700°C-600°C, respectively.

Declaration of Competing Interest

The authors declare that they have no known competing financial interests or personal relationships that could have appeared to influence the work reported in this paper.

Data Availability

Data will be made available on request.

Acknowledgements

The authors also acknowledge, with pleasure, support from the National Science Foundation (NSF) with NSF-PREM grant #DMR-1827745. This material is also based upon work supported by the Air Force Office of Scientific Research under award number FA9550-18-1-0387. However, any opinions, findings, and conclusions or recommendations expressed in this material are those of the author(s) and do not necessarily reflect the views of the United States Air Force.

References

[1] S.J. Pearton, J. Yang, P.H. Cary, F. Ren, J. Kim, M.J. Tadjer, M.A. Mastro, A review of Ga_2O_3 materials, processing, and devices, Appl. Phys. Rev. 5 (1) (2018), 011301, https://doi.org/10.1063/1.5006941.

[2] P. Jayaram, T.P. Jaya, S.Z. Karazhanov, P.P. Pradyumnan, Structural and physical property analysis of ZnO–SnO_2–In_2O_3–Ga_2O_3 quaternary transparent conducting oxide system, J. Mater. Sci. Technol. 29 (5) (2013) 419–422, https://doi.org/10.1016/j.jmst.2013.02.011.

[3] C. Xie, X. Lu, Y. Liang, H. Chen, L. Wang, C. Wu, D. Wu, W. Yang, L. Luo, Patterned growth of β-Ga_2O_3 thin films for solar-blind deep-ultraviolet photodetectors array and optical imaging application, J. Mater. Sci. Technol. 72 (2021) 189–196, https://doi.org/10.1016/j.jmst.2020.09.015.

[4] W. Choi, J. Ahn, K.T. Kim, H.J. Jin, S. Hong, D.K. Hwang, S. Im, Ambipolar channel p-TMD/n-Ga_2O_3 junction field effect transistors and high speed photo-sensing in TMD channel, Adv. Mater. (2021), e2103079, https://doi.org/10.1002/adma.202103079.

[5] W.Y. Kong, G.A. Wu, K.Y. Wang, T.F. Zhang, Y.F. Zou, D.D. Wang, L.B. Luo, Graphene-β-Ga_2O_3 heterojunction for highly sensitive deep UV photodetector application, Adv. Mater. 28 (48) (2016) 10725–10731, https://doi.org/10.1002/adma.201604049.

[6] N. Alfaraj, K.H. Li, M. Alawein, C.H. Kang, L. Braic, N.C. Zoita, A.E. Kiss, T.K. Ng, B. S. Ooi, Heteroepitaxial β-Ga_2O_3 on conductive ceramic templates: toward ultrahigh gain deep-ultraviolet photodetection, Adv. Mater. Technol. (2021), 210014, https://doi.org/10.1002/admt.202100142.

[7] Y. Zheng, M.N. Hasan, J.H. Seo, High-performance solar blind UV photodetectors based on single-crystal Si/β-Ga_2O_3 p-n heterojunction, Adv. Mater. Technol. 6 (6) (2021), 2100254, https://doi.org/10.1002/admt.202100254.

[8] Y. Xu, Y. Cheng, Z. Li, D. Chen, S. Xu, Q. Feng, W. Zhu, Y. Zhang, J. Zhang, C. Zhang, Y. Hao, Ultrahigh-performance solar-blind photodetectors based on high quality heteroepitaxial single crystalline β-Ga_2O_3 film grown by vacuumfree, low-cost mist chemical vapor deposition, Adv. Mater. Technol. 6 (6) (2021), 2001296, https://doi.org/10.1002/admt.202001296.

[9] T. Wang, H. Liang, Z. Han, Y. Sui, Z. Mei, Integrated flexible Ga_2O_3 deep UV photodetectors powered by environmental electromagnetic radiation energy, Adv. Mater. Technol. 6 (3) (2021), 2000945, https://doi.org/10.1002/admt.202000945.

[10] S. Salvatori, M. Girolami, P. Oliva, G. Conte, A. Bolshakov, V. Ralchenko, V. Konov, Diamond device architectures for UV laser monitoring, Laser Phys. (8) (2016) 26, https://doi.org/10.1088/1054-660X/26/8/084005.

[11] H. Umezawa, M. Nagase, Y. Kato, S.-i. Shikata, High temperature application of diamond power device, Diam. Relat. Mater. 24 (2012) 201–205, https://doi.org/10.1016/j.diamond.2012.01.011.

[12] J. Kim, M.A. Mastro, M.J. Tadjer, J. Kim, Heterostructure WSe_2−Ga_2O_3 junction field-effect transistor for low-dimensional high-power electronics, ACS Appl. Mater. Interfaces 10 (35) (2018) 29724–29729, https://doi.org/10.1021/acsami.8b07030.

[13] J. Ma, H.J. Cho, J. Heo, S. Kim, G. Yoo, Asymmetric double-Gate β-Ga_2O_3 nanomembrane field-effect transistor for energy-efficient power devices, Adv. Electron. Mater. 5 (6) (2019), 1800938, https://doi.org/10.1002/aelm.201800938.

[14] H. Zhou, K. Maize, J. Noh, A. Shakouri, P.D. Ye, Thermodynamic studies of β-Ga_2O_3 nanomembrane field-effect transistors on a sapphire substrate, ACS Omega 2 (11) (2017) 7723–7729, https://doi.org/10.1021/acsomega.7b01313.

[15] S. Manandhar, A.K. Battu, A. Devaraj, V. Shutthanandan, S. Thevuthasan, C. V. Ramana, Rapid response high temperature oxygen sensor based on titanium doped gallium oxide, Sci. Rep. 10 (1) (2020) 178, https://doi.org/10.1038/s41598-019-54136-8.

[16] E.J. Rubio, T.E. Mates, S. Manandhar, M. Nandasiri, V. Shutthanandan, C. V. Ramana, Tungsten incorporation into gallium oxide: crystal structure, surface and interface chemistry, thermal stability, and interdiffusion, J. Phys. Chem. C 120 (47) (2016) 26720–26735, https://doi.org/10.1021/acs.jpcc.6b05487.

[17] H. Dong, S. Pang, Y. Xu, Z. Li, Z. Zhang, W. Zhu, D. Chen, H. Xi, Z. Lin, J. Zhang, Y. Hao, C. Zhang, Ultrawide band gap oxide semiconductor-triggered performance improvement of perovskite solar cells via the novel Ga_2O_3/SnO_2 Composite electron-transporting bilayer, ACS Appl. Mater. Interfaces 12 (49) (2020) 54703–54710, https://doi.org/10.1021/acsami.0c16168.

[18] Z. Zhang, Z. Chen, M. Chen, K. Wang, H. Chen, S. Deng, G. Wang, J. Chen, ε-Ga_2O_3 thin film avalanche low-energy X-Ray detectors for highly sensitive detection and fast-response applications, Adv. Mater. Technol. 6 (4) (2021), 2001094, https://doi.org/10.1002/admt.202001094.

[19] H. Liang, S. Cui, R. Su, P. Guan, Y. He, L. Yang, L. Chen, Y. Zhang, Z. Mei, X. Du, Flexible X-ray detectors based on amorphous Ga_2O_3 thin films, ACS Photonics 6 (2) (2018) 351–359, https://doi.org/10.1021/acsphotonics.8b00769.

[20] M. Wurdack, T. Yun, E. Estrecho, N. Syed, S. Bhattacharyya, M. Pieczarka, A. Zavabeti, S.Y. Chen, B. Haas, J. Muller, M.N. Lockrey, Q. Bao, C. Schneider, Y. Lu, M.S. Fuhrer, A.G. Truscott, T. Daeneke, E.A. Ostrovskaya, Ultrathin Ga_2O_3 glass: a large-scale passivation and protection material for monolayer WS_2, Adv. Mater. 33 (3) (2021), e2005732, https://doi.org/10.1002/adma.202005732.

[21] K. Arora, N. Goel, M. Kumar, M. Kumar, Ultrahigh performance of self-powered β-Ga_2O_3 thin film solar-blind photodetector grown on cost-effective Si substrate using high-temperature seed layer, ACS Photonics 5 (6) (2018) 2391–2401, https://doi.org/10.1021/acsphotonics.8b00174.

[22] B. Mallesham, S. Roy, S. Bose, A.N. Nair, S. Sreenivasan, V. Shutthanandan, C. V. Ramana, Crystal chemistry, band-gap red shift, and electrocatalytic activity of iron-doped gallium oxide ceramics, ACS Omega 5 (1) (2020) 104–112, https://doi.org/10.1021/acsomega.9b01604.

[23] W. Zhang, B.S. Naidu, J.Z. Ou, A.P. O'Mullane, A.F. Chrimes, B.J. Carey, Y. Wang, S.Y. Tang, V. Sivan, A. Mitchell, S.K. Bhargava, K. Kalantar-Zadeh, Liquid metal/metal oxide frameworks with incorporated Ga_2O_3 for photocatalysis, ACS Appl. Mater. Interfaces 7 (3) (2015) 1943–1948, https://doi.org/10.1021/am5077364.

[24] Z. Guo, A. Verma, X. Wu, F. Sun, A. Hickman, T. Masui, A. Kuramata, M. Higashiwaki, D. Jena, T. Luo, Anisotropic thermal conductivity in single crystal β-Gallium Oxide, Appl. Phys. Lett. (11) (2015) 106, https://doi.org/10.1063/1.4916078.

[25] A.S. Pratiyush, S. Krishnamoorthy, S. Kumar, Z. Xia, R. Muralidharan, S. Rajan, D. N. Nath, Demonstration of zero bias responsivity in MBE grown β-Ga_2O_3 lateral deep-UV photodetector, Jpn. J. Appl. Phys. (6) (2018) 57, https://doi.org/10.7567/JJAP.57.060313.

[26] A.F.M. Anhar Uddin Bhuiyan, Z. Feng, J.M. Johnson, H.-.L. Huang, J. Hwang, H. Zhao, MOCVD epitaxy of ultrawide bandgap β$(Al_xGa_{1-x})_2O_3$ with high-Al composition on (100) βGa_2O_3 substrates, Cryst. Growth Des. 20 (10) (2020) 6722–6730, https://doi.org/10.1021/acs.cgd.0c00864.

[27] Z. Galazka, R. Uecker, K. Irmscher, M. Albrecht, D. Klimm, M. Pietsch, M. Brützam, R. Bertram, S. Ganschow, R. Fornari, Czochralski growth and characterization of β-Ga_2O_3 single crystals, Cryst. Res. Tech. 45 (12) (2010) 1229–1236, https://doi.org/10.1002/crat.201000341.

[28] N. Makeswaran, D. Das, V. Zade, P. Gaurav, V. Shutthanandan, S. Tan, C. V. Ramana, Size-and phase-controlled nanometer-thick β-Ga_2O_3 films with green photoluminescence for optoelectronic applications, ACS Appl. Nano Mater. 4 (4) (2021) 3331–3338, https://doi.org/10.1021/acsanm.1c00378.

[29] Y. Song, P. Ranga, Y. Zhang, Z. Feng, H.L. Huang, M.D. Santia, S.C. Badescu, C. U. Gonzalez-Valle, C. Perez, K. Ferri, R.M. Lavelle, D.W. Snyder, B.A. Klein, J. Deitz, A.G. Baca, J.P. Maria, B. Ramos-Alvarado, J. Hwang, H. Zhao, X. Wang, S. Krishnamoorthy, B.M. Foley, S. Choi, Thermal conductivity of βPhase Ga_2O_3 and $(Al_xGa_{1-x})_2O_3$ heteroepitaxial thin films, ACS Appl. Mater. Interfaces 13 (32) (2021) 38477–38490, https://doi.org/10.1021/acsami.1c08506.

[30] D. Das, F.S. Escobar, P.G. Nalam, P. Bhattacharya, C.V. Ramana, Excitation dependent and time resolved photoluminescence of β-Ga_2O_3, β-$(Ga_{0.955}Al_{0.045})_2O_3$ and β-$(Ga_{0.91}In_{0.09})_2O_3$ epitaxial layers grown by pulsed laser deposition, J. Lumin. 248 (2022), 118960, https://doi.org/10.1016/j.jlumin.2022.118960.

[31] C.H. Liang, G.W. Meng, G.Z. Wang, Y.W. Wang, L.D. Zhang, Catalytic synthesis and photoluminescence of β-Ga_2O_3 nanowires, Appl. Phys. Lett. 78 (2001) 3202, https://doi.org/10.1063/1.1374498.

[32] R. Sun, Y.K. Ooi, P.T. Dickens, K.G. Lynn, M.A. Scarpulla, On the origin of red luminescence from iron-doped β-Ga_2O_3 bulk crystals, Appl. Phys. Lett. 117 (5) (2020), 052101, https://doi.org/10.1063/5.0012967.

[33] M. Alonso-Orts, E. Nogales, J.M. San Juan, M.L. Nó, J. Piqueras, B. Méndez, Modal Analysis of β−Ga_2O_3: Cr widely tunable luminescent optical microcavities, Phys. Rev. Appl. 9 (6) (2018), 064004. https://link.aps.org/doi/10.1103/PhysRevApplied.9.064004.

[34] A.S. Pratiyush, S. Krishnamoorthy, S.V. Solanke, Z. Xia, R. Muralidharan, S. Rajan, D.N. Nath, High responsivity in molecular beam epitaxy grown β-Ga_2O_3 metal semiconductor metal solar blind deep-UV photodetector, Appl. Phys. Lett. 110 (22) (2017), 221107, https://doi.org/10.1063/1.4984904.

[35] Point defects in Ga_2O_3, J. Appl. Phys. 127 (10) (2020), 101101, https://doi.org/10.1063/1.5142195.

[36] M. Girolami, A. Bellucci, M. Mastellone, S. Orlando, V. Valentini, R.M. Montereali, M.A. Vincenti, R. Polini, D.M. Trucchi, Optical characterization of double-nanotextured black diamond films, Carbon 138 (2018) 384–389, https://doi.org/10.1016/j.carbon.2018.07.055.

[37] T. Luhmann, R. John, R. Wunderlich, J. Meijer, S. Pezzagna, Coulomb-driven single defect engineering for scalable qubits and spin sensors in diamond, Nat. Commun. 10 (1) (2019) 4956, https://doi.org/10.1038/s41467-019-12556-0.

[38] M. Jošt, S. Albrecht, L. Kegelmann, C.M. Wolff, F. Lang, B. Lipovšek, J. Krč, L. Korte, D. Neher, B. Rech, M. Topič, Efficient light management by textured nanoimprinted layers for perovskite solar cells, ACS Photonics 4 (5) (2017) 1232–1239, https://doi.org/10.1021/acsphotonics.7b00138.

[39] I. Hwang, D. Choi, S. Lee, J.H. Seo, K.H. Kim, I. Yoon, K. Seo, Enhancement of light absorption in photovoltaic devices using textured polydimethylsiloxane stickers, ACS Appl. Mater. Interfaces 9 (25) (2017) 21276–21282, https://doi.org/10.1021/acsami.7b04525.

[40] G. Gutierrez, E.M. Sundin, P.G. Nalam, V. Zade, R. Romero, A.N. Nair, S. Sreenivasan, D. Das, C. Li, C.V. Ramana, Interfacial phase modulation-induced structural distortion, band gap reduction, and nonlinear optical activity in Tin-incorporated Ga_2O_3, J. Phys. Chem. C 37 (2021) 20468–20481, https://doi.org/10.1021/acs.jpcc.1c04005.

[41] L. Binet, D. Gourier, Origin of the blue luminescence of β-Ga_2O_3, J. Phys. Chem. Solids 59 (8) (1998) 1241–1249, https://doi.org/10.1016/S0022-3697(98)00047-X.

[42] A. Aiello, D. Das, P. Bhattacharya, InGaN/GaN quantum dot light-emitting diodes on silicon with coalesced GaN nanowire buffer layer, ACS Appl. Nano Mater. 4 (2021) 1825–1830, https://doi.org/10.1021/acsanm.0c03227.

[43] K.M. Othonos, M. Zervos, C. Christofides, A. Othonos, Ultrafast spectroscopy and red emission from β-Ga_2O_3/β-Ga_2S_3 nanowires, Nanoscale Res. Lett. 10 (1) (2015) 1016, https://doi.org/10.1186/s11671-015-1016-y.

[44] A. Aiello, Y. Wu, A. Pandey, P. Wang, W. Lee, D. Bayerl, N. Sanders, Z. Deng, J. Gim, K. Sun, R. Hovden, E. Kioupakis, Z. Mi, P. Bhattacharya, Deep ultraviolet luminescence due to extreme confinement in monolayer GaN/Al(Ga)N nanowire and planar heterostructures, Nano Lett. 19 (11) (2019) 7852–7858, https://doi.org/10.1021/acs.nanolett.9b02847.